Journal of Solid State Chemistry 341 (2025) 125050

Contents lists available at ScienceDirect

Journal of Solid State Chemistry

journal homepage: www.elsevier.com/locate/jssc

Synthesis of double carbide (Ti,Cr)C with a different Cr content produced by electro thermal explosion

I.I. Chuev [a,*], D. Yu Kovalev [a], A.V. Scherbakov [a], S.A. Guda [b]

[a] Merzhanov Institute of Structural Macrokinetics and Materials Science, Russian Academy of Sciences, Chernogolovka, Moscow Region 142432, Russia
[b] SFU, 178/24 Andrey Sladkov Str., Rostov on Don 344090, Russia

ARTICLE INFO

Keywords:
Double carbide (Ti,Cr)C
Electro thermal explosion
DFT calculations

ABSTRACT

In this paper we report the preparation of double carbide (Ti,Cr)C with a chromium content of 10 ÷ 30 at% by electrothermal explosive synthesis (ETE). This method allows synthesis to be carried out at high temperature with minimal holding time. The ETE method is favourable for the formation of dense carbide ceramics. The synthesized samples were characterized by X-ray diffraction and scanning electron microscopy. It was found experimentally that the unit cell parameter of the double carbide decreases linearly with increasing chromium content. The DFT calculations also confirmed the dependence of the unit cell parameter (Ti,Cr)C on the chromium content according to Vegard's law and show changes in the cell shape and distance between Cr–Cr layers with increasing chromium content. The pDOS diagram shows that an increase in chromium content leads to an excess of d* electrons on the π* orbitals, which has a destabilizing effect on the double carbide structure.

Crystal Orbital Hamiltonian (COHP) analysis of the electronic structure of the double carbide, partitioning the energy of the band structure into bonding, non-bonding and anti-bonding energy regions, showed the influence of chromium content on its stability.

1. Introduction

Refractory transition metal carbides such as titanium carbide are valuable materials for high temperature applications due to their excellent properties. The addition of alloying elements to form solid solutions such as (Ti,M)C can improve the strength and properties of the material. The alloying element M acts as a strengthening element, improving the double carbides (Ti,W)C, (Ti,V)C, (Ti,Zr)C and (Ti,Cr)C [1–4] and their overall performance. This strategy has been successfully demonstrated with different carbide combinations. The viscosity and toughness of the cemented carbide can be improved, extending its potential applications in high stress environments.

The use of chromium as an alloying element can increase the strength and hardness of an alloy, making it more suitable for applications where durability and wear resistance are required [5]. It can also improve the impact strength of the alloy, which is important in applications where materials are subjected to sudden or intense loads. In addition, Cr can improve the corrosion resistance of the alloy by forming a protective oxide layer on the surface, which helps to prevent rust and other forms of corrosion. Control of the synthesis conditions is essential to achieve the desired Cr content in double carbide materials.

The range of chromium content in double carbide under equilibrium conditions is typically between 5 % and 15 % [6–8], with the exact value being strongly influenced by the specific synthesis conditions, in particular the temperature and duration of the heat treatment. Variations in these parameters can result in significant differences in the chromium content incorporated into a double carbide structure. The formation of double carbides under non-equilibrium conditions offers a wide range of interesting properties and applications.

Widely used synthesis methods such as spark plasma sintering (SPS) [1], self-propagating high-temperature synthesis (SHS) [9] and electrothermal explosion (ETE) [10,11] are all advanced techniques that allow the synthesis of materials with unique properties.

The ETE method is a promising technique for the synthesis of ceramic materials and the study of the formation mechanism of heterogeneous condensed systems under extreme conditions. It allows the investigation of structural features in materials such as cemented carbides at high temperatures (2500K) and short reaction times (1min). Compared to SPS and SHS, the ETE method provides extreme experimental conditions to produce dense ceramics in a single stage. Overall, manipulation of chromium content and synthesis conditions can play an important role in tailoring the properties of alloys for specific applications.

* Corresponding author.
E-mail address: ichuev@ism.ac.ru (I.I. Chuev).

https://doi.org/10.1016/j.jssc.2024.125050
Received 2 August 2024; Received in revised form 25 September 2024; Accepted 13 October 2024
Available online 16 October 2024

Table 1
Green mixture composition.

Sample	Content, at.%			Formula
	Ti	Cr	C	
1	40	10	50	$Ti_{0.4}Cr_{0.1}C$
2	30	20	50	$Ti_{0.3}Cr_{0.2}C$
3	20	30	50	$Ti_{0.2}Cr_{0.3}C$
4	10	40	50	$Ti_{0.1}Cr_{0.4}C$

Thus this work contributes to the fundamental understanding of (Ti, Cr)C double carbides and provides valuable information for optimizing their properties for specific applications in the field of materials science and engineering.

2. Experimental

2.1. Materials

The starting materials were prepared from a mixture of commercial powders of chromium (brand PX-1M, 99.35 % pure, particle size <70 μm), titanium (brand PTS, 99.0 % pure, particle size 30–45 μm) and carbon (brand P803T, 99.0 % pure, particle size <1 μm). The composition of the mixture was chosen to obtain the ratios between the reagents as indicated in Table 1. The powders were mixed in a ball mill for 1 h. The powder mixtures were pressed into cylindrical samples (weight 5 g, diameter 12 mm, height 17 mm) with a relative density of 0.6.

2.2. Electrothermal explosion (ETE)

The synthesis of the (Ti,Cr)C double carbides was carried out using the ETE method. ETE is a one-step method for the preparation of compact high-temperature ceramics. The synthesis scheme and experimental setup are described in detail in Refs. [11–13].

The essence of the method is the heating of the reaction sample by direct passage of electric current. Rapid heating causes exothermic interaction of the reagents, resulting in ignition of the entire sample. The high synthesis temperature ensures a short sintering time for the reaction product. A required condition for an ETE is high electrical conductivity and mechanical strength of the sample, pressed from a reacting mixture of powders, to ensure rapid heating and prevent fracture due to impurity gases released during the exothermic reaction. Uniform heating of samples at extremely high rates (up to 10^5 s^{-1}) is achieved.

The experimental facility (Fig. 1) consists of a reaction press mould (35 mm in diameter and 100 mm in height), a current transformer, a power controller and a system for determining the electrical and thermal parameters of the ETE, including a measurement bus and an analogue-to-digital converter. A cylindrical sample is placed between a punch electrode and a mould base. A cylindrical sample is placed between a punch electrode and a mould base. A TiC powder is applied to the top and bottom of the sample to provide a galvanic connection to the punch electrode and mould base and to protect them from high temperatures. The space between the cylindrical surface of the sample and the wall of the press mould is filled with SiO_2 powder with a particle size of 200–300 μm. The dielectric dispersion medium ensures quasi-static compression of the sample and removal of the impurity gas released during the exothermic reaction. The reaction press mould containing the sample is placed on the worktable of a pneumatic press and connected to

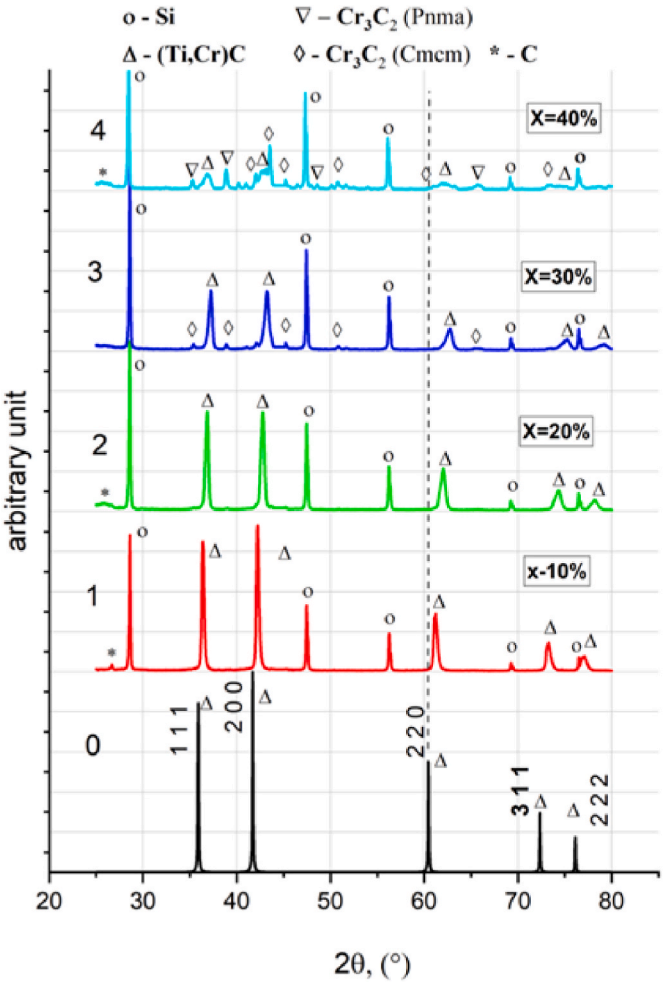

Fig. 2. XRD patterns (1–4) of the synthesized samples with different Cr content (X = 10–40 at.%). (0) – reference pattern of TiC (PDF2 #01-073-0472).

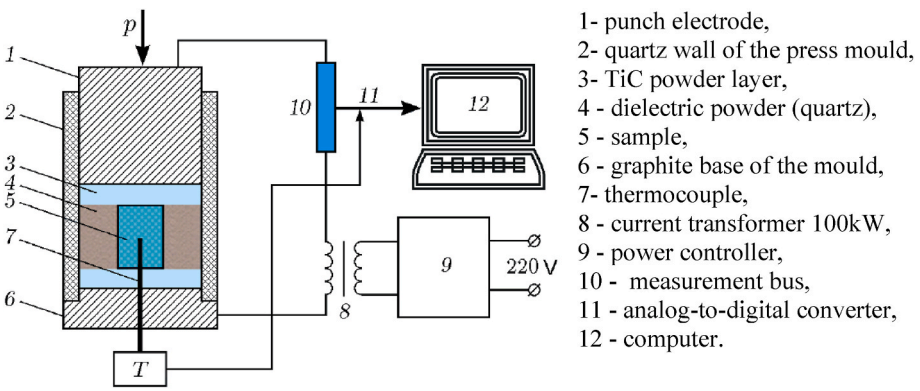

Fig. 1. Schematic diagram of the experimental setup.

Table 2
Phase composition (wt %) of samples after ETE synthesis.

N°	Cr content in the green mixture X at. %	Double carbide phase		Cr_7C_3 Pnma	Cr_3C_2		C $P6_3mmc$	R_{wt}/GOF %
		(TiCr)C1 Fm-3m	(TiCr)C2 Fm-3m		Pnma	Cmcm		
1	10	41.8 (5)	51.1 (2)	1.8 (2)	0	2.1 (2)	3.2 (2)	8.9/1.7
2	20	25.8 (4)	66.5 (4)	0	0	5.2 (2)	2.5 (1)	9.0/1.4
3	30	37.9 (2)	49.2 (3)	0	0	12.8 (2)	0	7.8/1.3
4	40	17.7 (3)	28.8 (7)	0	16.7 (5)	36.8 (3)	0	9.2/1.5

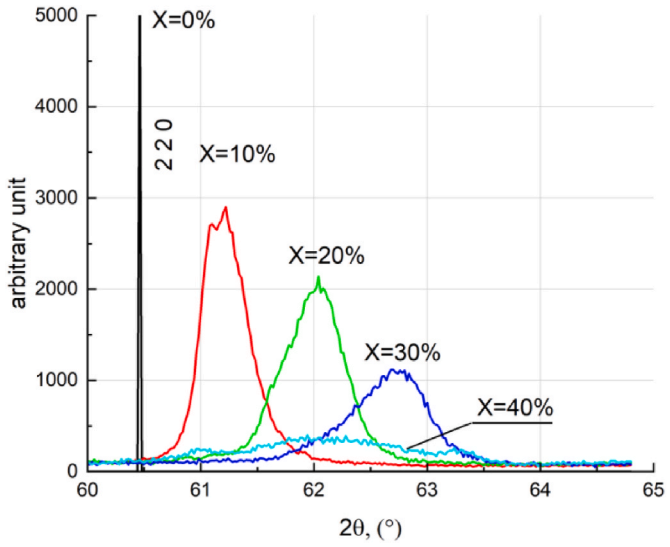

Fig. 3. Displacement of $(Ti_{1-x}Cr_x)C$ the (220) peak depending on the Cr content. To assess the sample composition (x = 40 %) scaled (I*10) values of Cr_3C_2 peaks in the spectrum was used.

the current transformer. After applying an axial load, the electrical voltage is applied and the sample is heated to ignition.

The effectiveness of the ETE method is highly dependent on the two main synthesis parameters - the electrical voltage applied to the sample and the pressure applied to the punch electrode. The choice of the synthesis parameters was based on our experimental data for samples with close electrical resistivity and dimensions. Based on the results of our previous work on the synthesis of carbide ceramics [11–13] and the results of preliminary experiments, the optimum synthesis parameters were determined - voltage 10 V, punch load 0.1 bar. The synthesis process can be divided into two stages. In the first stage, the sample was heated at a rate of 50 K/s until ignition. As the reaction progressed, the electrical resistance of the sample decreased and the electrical current increased from 100 to 2000 A. The maximum temperature of the thermal explosion was about 2500 K. In the second stage, the sample was sintered for 1 min while the electrical parameters remained practically unchanged.

2.3. Scanning electron microscopy

The morphology of the samples after ETE was examined using a Zeiss Ultra plus field emission scanning electron microscope based on the Ultra 55 (Carl Zeiss AG, Germany) equipped with an INCA 300 energy dispersive X-ray (EDX) analysis attachment. Electron micrographs were taken at electron beam acceleration voltages of 20 kV. EDX analysis for the carbide phase (TiCr)C was performed on 10 points and the results were averaged.

2.4. X-ray diffraction

After ETE, (Ti,Cr)C samples with different Cr contents were characterized by XRD (X-ray diffraction) using a diffractometer (DRON-3M, Bourevestnik, Russia) with CuKα radiation (λ = 1.54187 Å). The XRD patterns were scanned from 25° to 80° (2Θ) in a step scan mode with a scan increment of 0.02° and an exposure time of 10 s. To improve the accuracy of the unit cell parameter determination, the internal standard method was used with Si (NIST SRM 640b). Fitting the XRD patterns by the Rietveld refinement was made with Jana2006 [14] software using asymmetric pseudo-Voigt functions. The background, zero shift, profile parameters of the diffraction maxima, unit cell parameters, and phase content were refined. The structural parameters (site occupancy, atomic coordinates and thermal factors) of the phases were not refined. The $(Ti_{1-x}Cr_x)C$, Cr_3C_2 and Cr_7C_3 carbides were assumed to be carbides with stoichiometric C content. Profile decomposition of the (220) and (311) (Ti1-xCrx)C diffraction maxima was performed using the LIPRAS program [15].

2.5. Quantum chemical calculations

DFT calculations (VASP 6.3.0 software [16]) were performed with a plane-wave energy cutoff of 540 eV and a force-convergence tolerance of 0.01 eV/Å. Formation energies were calculated using the r2 SCAN metaGGA function, which improves the accuracy of reported thermodynamic data [17]. The self-consistent field was converged to at least 10-6 eV using an 8 × 8 × 8 k grid. The energies of the mixed carbides were calculated using a special quasirandom structure (SQS) supercell of 40 atoms [18].

Crystal Orbital Hamiltonian (COHP) analysis was performed using LOBSTER software [19,20], which partitioned the band structure energy (in terms of orbital pair contributions) into bonding, non-bonding and anti-bonding energy regions within a given energy range.

3. Results and discussion

3.1. XRD study

Fig. 2 shows the room temperature XRD patterns of the samples 1–4 with different Cr contents. The XRD pattern of TiC (PDF2 #01-073-0472) is shown for comparison. The XRD results indicate the presence of several phases, including (TiCr)C, Cr_7C_3, and Cr_3C_2. The results of a quantitative phase analysis using Rietveld refinement are shown in Table 2.

The main phase of samples 1–3 is the double carbide phase $(Ti_{1-x}Cr_x)C$ (Fm-3m), whose diffraction peaks are shifted with respect to those of TiC. As the Cr content increases, an increase in the content of the chromium carbide Cr3C2 is observed. At the maximum Cr content (sample 4), the synthesis leads to the formation of mainly Cr_3C_2 chromium carbide and the content of the double carbide $(Ti_{1-x}Cr_x)C$ decreases significantly.

A noticeable shift of $(Ti_{1-x}Cr_x)C$ peaks towards larger angles (Fig. 2) indicates a decrease in unit cell parameters, which is associated with an increase in Cr content in the crystal structure of $(Ti_{1-x}Cr_x)C$. The atomic radius of Cr (1.249 Å) [21] is significantly smaller than that of Ti (1.462

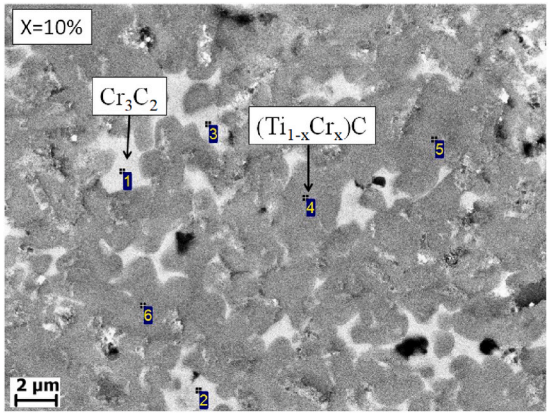

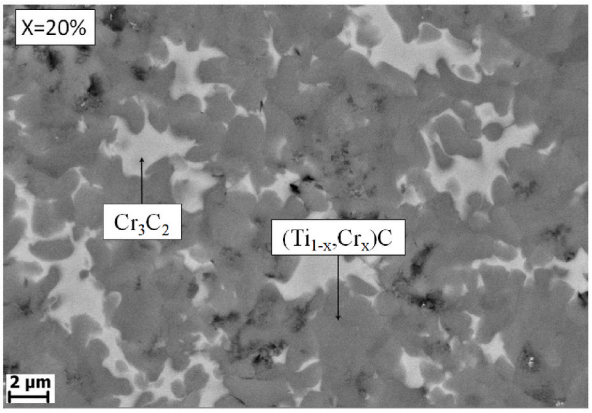

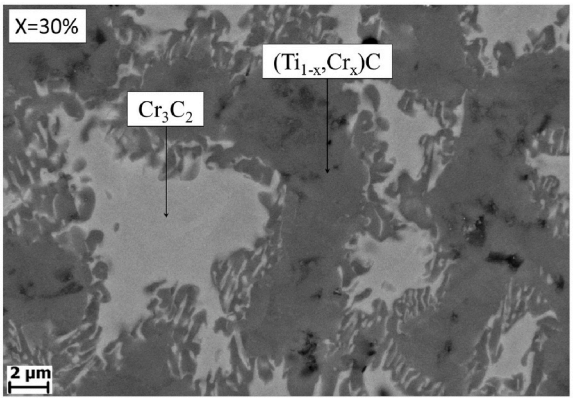

Spectrum	C	Ti	Cr
1	47.11	8.73	44.16
2	43.72	14.28	42.01
3	45.14	12.27	42.59
4	54.95	25.60	19.45
5	50.63	32.49	16.88
6	56.51	28.17	15.32

Fig. 4. SEM micrographs for samples 1–3 with different Cr content (X = 10–30 at. %) and EDX analysis for sample 1 (X = 10 at. %).

Table 3
Cr content (at.%) in double carbide $(Ti_{1-x}Cr_x)C$ from EDX and XRD analysis.

Analysis	Cr content in the green mixture, X at.%					
	10		20		30	
EDX	10.2 ± 1.4		16.8 ± 1.6		23.8 ± 3.2	
XRD[a]	(TiCr)C 1	(TiCr)C 2	(TiCr)C 1	(TiCr)C 2	(TiCr)C 1	(TiCr)C 2
	8.9	11.5	16.5	20.0	23.3	28.9

[a] The chromium content in the (TiCr)C 1 and (TiCr)C 2 phases was calculated using the Vegard's law, equation (1).

Å) and the unit cell parameter decreases when Ti atoms are replaced. At the maximum Cr content in the green mixture (40 at.%), the intensity of the (220) peak decreases significantly and its position shifts towards higher angles, indicating that the synthesized sample (4) is saturated with Cr atoms (Fig. 3).

3.2. Electron microscopy

Micrographs of samples (1–3) show the presence of two structural components - rounded grains of double carbide $(Ti_{1-x}Cr_x)C$ (dark areas) and chromium carbides (light areas) (Fig. 4). According to the EDX analysis data, the chromium content in the double carbide increases with increasing chromium content in the green mixture (Table 3). The results of the EDX measurements represent an integral evaluation of the chromium content in the (TiCr)C 1 and (TiCr)C 2 phases. The Cr content values obtained from the EDX measurements are close to the chromium content in the (Ti,Cr)C 1 and (TiCr)C 2 phases calculated using Vegard's law. In the double carbide the carbon content is close to stoichiometric (Fig. 4).

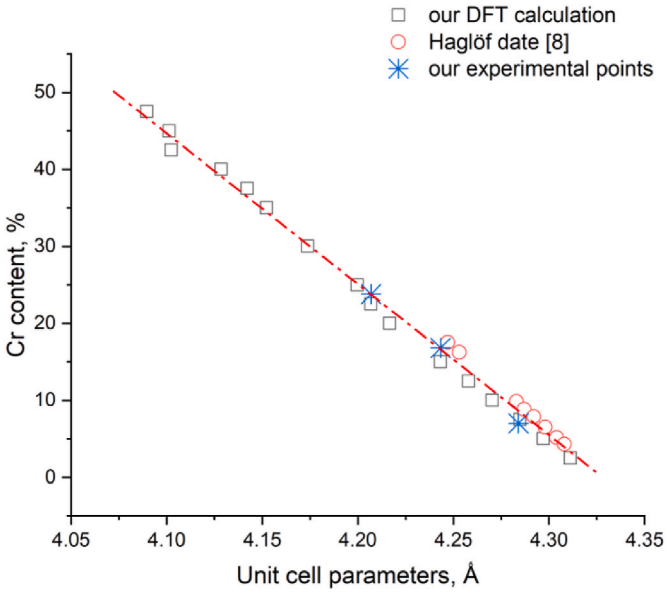

Fig. 5. Dependence of Cr content vs unit cell parameters.

According to Ref. [8] the wavelength-dispersive spectroscopy analysis confirms the stoichiometry of carbon at the equilibrium concentration of Cr in the range of 5–15 %. Comparison of the straight lines plotted according to Vegard's law shows a complete agreement of the data between the Haglöf plotted lines the points based on DFT calculations (red circle dots) and on the experimental data (blue star dots)

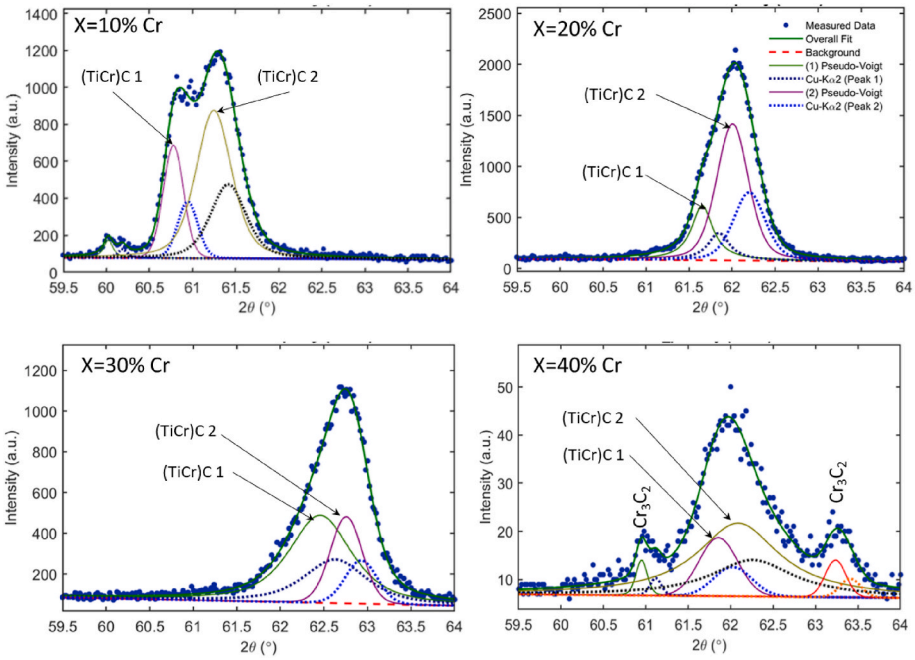

Fig. 6. Profile of (220) $(Ti_{1-x}Cr_x)C$ diffraction maximum for different Cr contents. The profiles are shown as two pseudo-Voigt peaks. The solid lines are numbered constituent peaks. The positions of the peaks for Cu $K_{\alpha 2}$ radiation are indicated by dots.

(Fig. 5). Considering that the carbon concentration affects the lattice parameter [22], it is possible to make a statement about the stoichiometry of carbon in double carbide.

3.3. Profile of the double carbide peaks. Quantum chemical clarification Vegard's law

The shape of the profile of the double carbide $(Ti_{1-x}Cr_x)C$ peaks indicates their asymmetry and the possibility of representing the profile as two pseudo-Voigt peaks. Peaks (220) and (311) were selected for profile analysis. They were located at the far angles, with minimal overlap between the double carbide peaks and the chromium carbide peaks (Fig. 6). The profiles for the (311) peaks are not shown as they are similar to the (220) peaks. According to the data obtained, the mixture consists of two double carbide phases with different chromium contents. In Fig. 6, Tables 3 and 5 these phases are labelled as (TiCr)C 1 and (TiCr)C 2. Additional peaks at ~61° and 63° (Fig. 6, X = 40 %) correspond to chromium carbide Cr_3C_2.

Based on the data in Tables 3 and 5, the relationship between the weighted average of the $(Ti_{1-x}Cr_x)C$ unit cell parameters and the mean value of the chromium content obtained from the EDX analysis was plotted (Fig. 5). In the graph, these experimental data are represented by the star dots (x). The results for the (TiCr)C carbide, as reported by Haglöf et al. [8], are represented by the circle dot (o).

The experimental data obtained are in good agreement with Vegard's law, which allows us to establish a correspondence between the unit cell parameters and the chromium content in the double carbide $(Ti_{1-x}Cr_x)C$. By approximating the experimental data of unit cell parameter (a) vs. Cr content (at. % Cr) with a linear function, the following equations are obtained:

$$\%Cr = 851(3) - 196.5(7)\cdot a(Å) \quad (1)$$

Statistical analysis of the experimental points in Fig. 5, when described by a linear function, gives a value of $R^2 = 0.99996$. The value of the statistical parameter for Vegard's law indicates a high degree of agreement with the linear dependence.

DFT calculations were carried out for structures with a given Cr content to clarify the data from Vegard's law. A straight line is used to illustrate the calculated dependence of the chromium content in double carbide on the unit cell parameters (□) (Fig. 5). The calculated values are in good agreement with our experimental data.

3.4. Quantum chemical study of double carbide stability

DFT calculations of the crystal structure without symmetry restriction show changes in the shape and distance between the Cr–Cr layers of the unit cell as the chromium content increases (Fig. 7).

The stability of double carbide is determined by the ability of the compound to relax under impact while maintaining the crystal structure unchanged. DFT calculations showed that dense layers of chromium atoms form in the crystal structure of the double carbide.

The distance between adjacent layers in Cr–Cr stacks is given in Table 4. Changes in the chromium content are associated with non-monotonic changes in the shape of the crystal and consequently with a change in the distance between Cr–Cr layers. Thus, increasing the chromium concentration till 25 % leads to an increase in the Cr–Cr distance between the atoms in the stacks and consequently to an increase in their mobility. At Cr contents of 10 and 20 %, the small distances can be relaxed by the displacement of the double carbides of the plane parallel to the stacks, which favours the mobility of the chromium atoms.

The enthalpy of double carbide formation was calculated using the DFT method as a function of chromium content. The results are shown in Fig. 8. The lower enthalpy of formation at higher chromium concentrations in double carbides indicates that the presence of chromium destabilizes the (Ti,Cr)C crystal structure.

From Fig. 9 it can be seen that the Fermi level and the partial density diagram (pDOS) intersect at a point and its value depends on the chromium content in the double carbide. Increasing the chromium content results in an excess of d-electrons. These additional d-electrons occupy the unfilled chromium (Cr) orbitals and can affect the electronic structure and properties of the material. pCOHP analysis of the Ti–Cr and

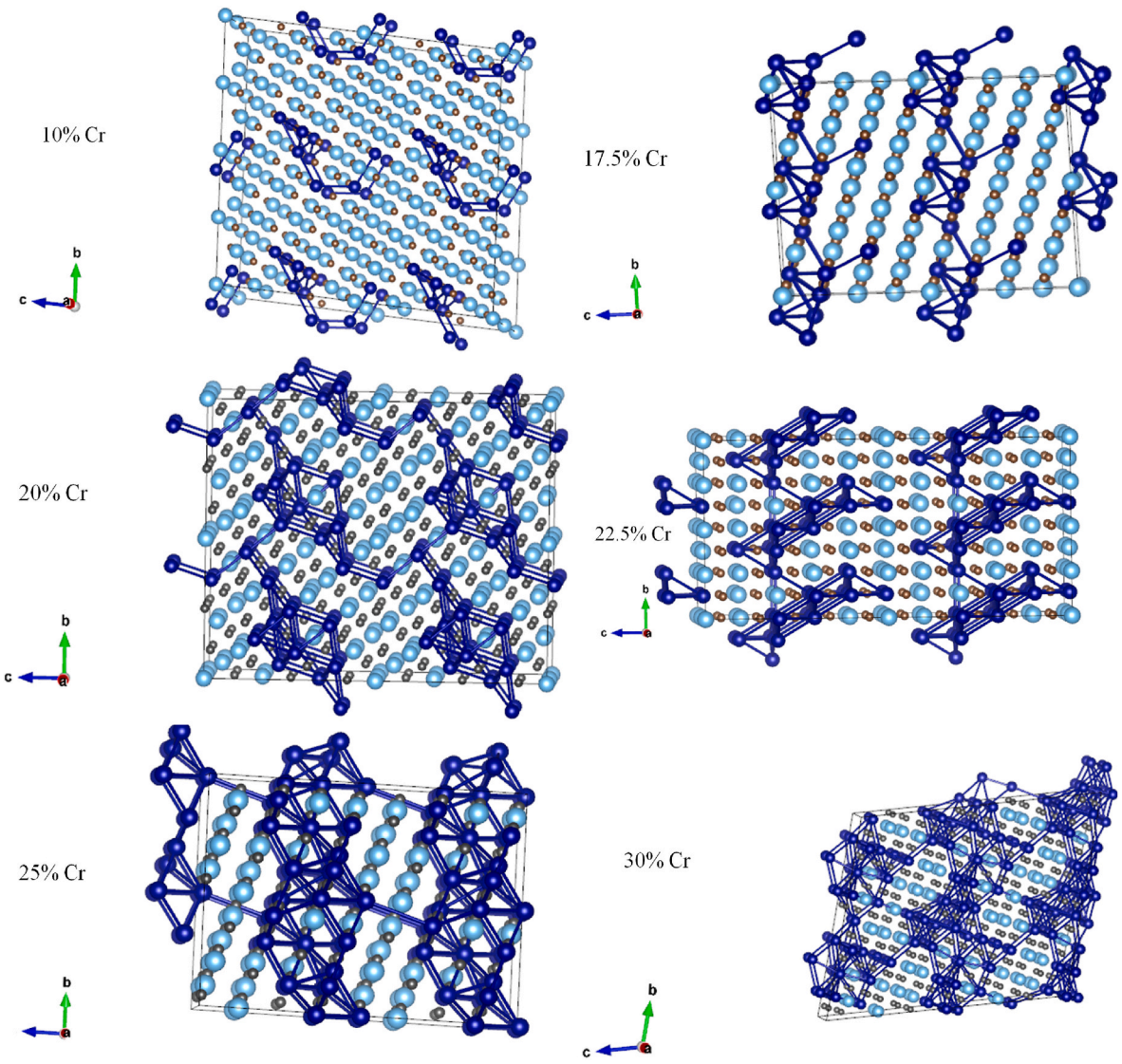

Fig. 7. Cell shape of double carbide (Ti,Cr)C with different chromium content obtained from DFT calculations. Mark atoms with circles (Cr is dark blue, Ti is light blue, carbon is black) Vesta software [23].

Table 4
Changes in the distance between the Cr–Cr layers and the cell shape of the double carbide (Ti,Cr)C with increasing chromium content.

Cr at.%	γ[a], deg.	Distance between Cr–Cr layers, Å[b]	Density, g/cm^2
10	80.4	5.309	5.03
17.5	72.5	6.849	5.09
20	89.9	5.17	5.15
22.5	90	6.126	5.18
25	72.4	6.66	5.17
30	95	5.081	5.22

[a] γ - is the angle between axes *c* and *b*. The axis *a* is perpendicular to the plane of the figure.

[b] Distance between Cr–Cr layers - shortest distance between symmetrically connected chromium atoms.

Cr–Cr bonds is shown in Fig. 10.

The pDOS diagram shows that an increase in chromium content leads to an excess of d* electrons on the π* orbitals (Fig. 9). This has a destabilizing effect on the double carbide structure. The repulsive interaction between Cr(π)-Cr leads to destabilization of the double carbide crystal structure.

Table 5
Unit cell parameters of $(Ti_{1-x}Cr_x)C$.

Double carbide phase	Cr content in the green mixture, X at. %			
	10	20	30	40
(TiCr)C 1	4.2965 (2)	4.2578 (1)	4.2228 (5)	4.2234 (3)
(TiCr)C 2	4.2834 (9)	4.2396 (2)	4.1946 (3)	4.1954 (4)
Weighted average value	4.2860 (1)	4.2442 (3)	4.2070 (1)	4.2059 (1)

Let's consider the Ti–Cr bond. At Cr contents up to 25 %, Ti–Cr d-electrons appear in the bonding region, strengthening the Ti–Cr bond. Further increase in Cr content >30 % leads to the population of the d-antibonding orbital, weakening the Ti–Cr interaction.

As for the Cr–Cr bond, binding interactions of Cr–Cr occur at Cr contents of less than 10 %. A subsequent increase in Cr content (>25 %) leads to an insignificant population of the d-antibonding orbital. A further increase in Cr content (30 %) leads to a significant

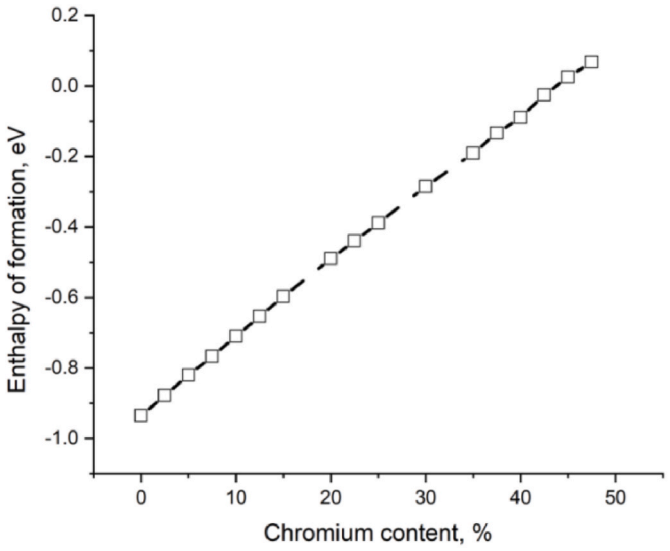

Fig. 8. Dependence of enthalpy of $(Ti_{1-x}Cr_x)C$ formation on chromium content.

destabilization of the double carbide. Thus, the chromium content plays an important role in the stability of the double carbide $(Ti_{1-x}Cr_x)C$. Joint pCOHP analysis of the Cr–Cr and Ti–Cr bonds provides an opportunity to evaluate the chromium content (25 at.%), allowing a distinction to be made between a stable carbide and an unstable one.

4. Conclusion

1. The double carbide with a chromium content of 10 ÷ 30 at% (Ti,Cr)C was prepared by electrothermal explosive synthesis. The ETE technique makes it possible to obtain dense carbide ceramics in a single technological step with minimum dwell time at high temperature. The essence of the ETE method is the heating of the reaction sample by direct passage of electric current. Rapid heating causes exothermic interaction of the reagents, resulting in ignition of the entire sample.
2. The unit cell parameter of the double carbide (Ti,Cr)C decreases linearly with increasing chromium content. The experimental data are in good agreement with Vegard's law and by approximating the data with a linear function, the following equations are obtained:

%Cr = 851(3) - 196.5(7)·a(Å)

The DFT calculations also confirmed the linear dependence of the unit cell parameter (Ti,Cr)C on the Cr content and show changes in the cell shape and the distance between the Cr–Cr layers of the unit cell with increasing chromium content.

3. The pDOS diagram shows that an increase in chromium content leads to an excess of d* electrons on the π* orbitals, which has a destabilizing effect on the double carbide structure.

The pCOHP analysis also showed that the occupancy of d-electrons near the Fermi level, including the Cr (d*) antibonding orbitals, affects the stability of the double carbide structure.

The weakening of the Ti–Cr and Cr–Cr bonds in the double carbide sublattice within the (Ti, Cr)C compound can lead to the breakdown of the Ti and Cr framework.

CRediT authorship contribution statement

I.I. Chuev: Writing – original draft, Formal analysis, Data curation. **D. Yu Kovalev:** Writing – review & editing, Supervision, Conceptualization. **A.V. Scherbakov:** Methodology. **S.A. Guda:** Software.

Funding

This work was supported by the Ministry of Science and Higher Education of the Russian Federation in the framework of the State assignment of ISMAN (state registration No 122032900050–6).

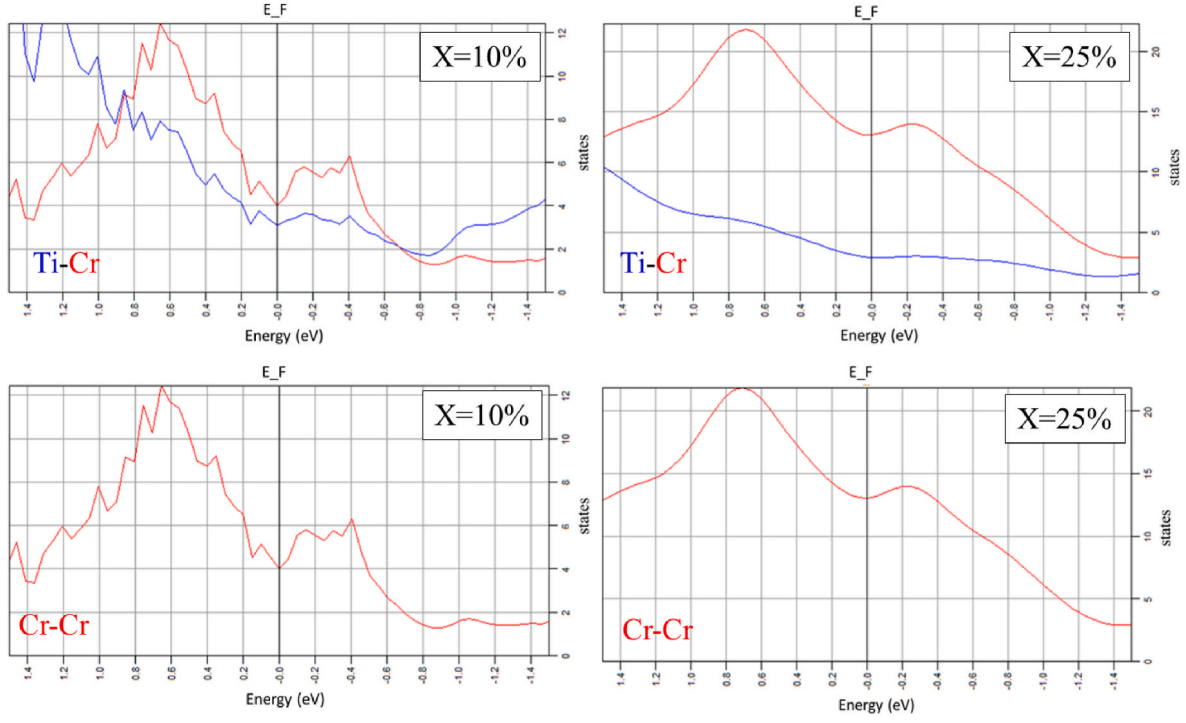

Fig. 9. Projected density of states of Ti - Cr and Cr – Cr atoms on d-orbital. E_F - Fermi level.

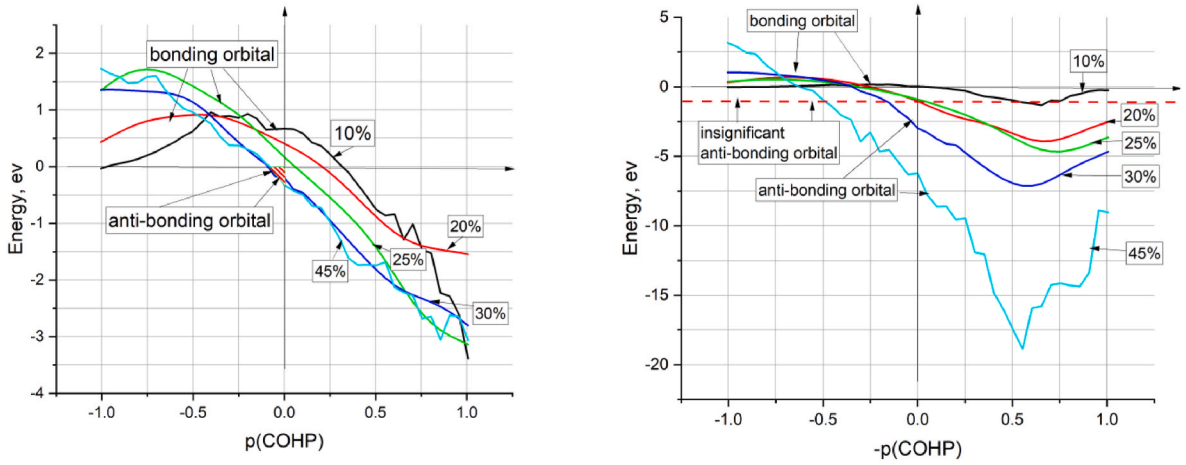

Fig. 10. PCOHP diagrams for Ti–Cr and Cr–Cr bonds depending on Cr content.

Declaration of competing interest

The authors declare that they have no known competing financial interests or personal relationships that could have appeared to influence the work reported in this paper.

Acknowledgements

This research was performed by using the set of modern scientific instruments available for multiple accesses at the ISMAN Centers of Shared Services.

Data availability

Data will be made available on request.

References

[1] H. Kwon, S.-A. Jung, W. Kim, Ti,Cr)C synthesized in situ by spark plasma sintering of TiC/Cr_3C_2 powder mixtures, Mater. Trans. 56 (2015) 264–268, https://doi.org/10.2320/matertrans.M2014327.

[2] A. Shmatov, L. Soos, Z. Krajny, Process for Producing Diamond-like carbode coatings on hard alloys, MM Science Journal 6 (2019) 2887–2890, https://doi.org/10.17973/MMSJ.2019_06_201812.

[3] X. Guo, X. Xin, W. Bao, X. Wang, Q. Yang, Y. Zeng, G. Zhang, Fa Xu, High hardness (Ti,Zr)C ceramic with dislocation networks, J. Am. Ceram. Soc. 105 (2022) 5515–5994, https://doi.org/10.1111/jace.18552.

[4] Z. Wang, D. Huo, Y. Zhou, G. Sui, F. Jiang, Effect of tungsten addition on continuous cooling transformation and precipitation behavior of a high titanium microalloyed steel, Metals 12 (2022) 1649, https://doi.org/10.3390/met12101649.

[5] I. Shon, H. Oh, J. Lim, H. Kwon, Mechanical properties and consolidation of binderless nanostructured (Ti,Cr)C from mechanochemically synthesized powder by high-frequency induction heating sintering, Ceram. Int. 39 (2013) 9721–9726, https://doi.org/10.1016/j.ceramint.2013.04.053.

[6] P. Booker, A. Kunrath, M. Hepworth, Experimental determination of the ternary diagram of the Ti–Cr–C system, Acta Mater. 45 (1997) 1625–1632, https://doi.org/10.1016/S1359-6454(96)00266-2.

[7] A. Ehrenborg, Investigation of the Cr Solubility in the MC Phase, Master thesis, 2016 921311 diva2.

[8] F. Haglöf, B. Kaplan, S. Norgren, et al., Experimental study of carbides in the Ti–Cr–C system, J. Mater. Sci. 54 (2019) 12358–12370, https://doi.org/10.1007/s10853-019-03810-3.

[9] W.N. Zhang, H.Y. Wang, P.J. Wang, J. Zhang, L. He, Q.C. Jiang, Effect of Cr content on the SHS reaction of Cr–Ti–C system, J. Alloys Compd. 465 (2008) 127–131, https://doi.org/10.1016/j.jallcom.2007.10.092.

[10] V.A. Knyasik, A.S. Shteinberg, V.I. Gorovenko, Thermal analysis of high-speed high-temperature reactions of refractory carbide synthesis, J. Therm. Anal. 40 (1993) 363–371, https://doi.org/10.1007/BF02546588.

[11] V.A. Shcherbakov, A.N. Gryadunov, I.E. Semenchuk, G.R. Nigmatullina, A. E. Sytschev, M.I. Alymov, The influence of mechanical activation on the structure and phase formation of an electro-thermal explosion in the Ti–Zr–C system, Ceram. Int. 49 (2023) 20017–20023, https://doi.org/10.1016/j.ceramint.2023.03.123.

[12] A.V. Shcherbakov, V.A. Shcherbakov, TaC by electrothermal explosion under pressure, Int. J. Self-Propag. High-Temp. Synth. 29 (2020) 122–123, https://doi.org/10.3103/S1061386220020119.

[13] V.A. Shcherbakov, A.V. Shcherbakov, A. S, Bostandzhiyan electrothermal explosion of a titanium—soot mixture under quasistatic compression. I. Thermal and electric parameters, Combust. Explos. Shock Waves 55 (2019) 74–81, https://doi.org/10.1134/S0010508219010088.

[14] V. Petricek, M. Dusek, L. Palatinus, Crystallographic computing system JANA2006: general features, Z. Kristallogr. 229 (2014) 345–352, https://doi.org/10.1515/zkri-2014-1737.

[15] G. Esteves, K. Ramos, C.M. Fancher, J.L. Jones, LIPRAS: Line-Profile Analysis Software, 2017, 0.13140/RG.2.2.29970.25282/3.

[16] G. Kresse, J. Furthmuller, Efficiency of ab-initio total energy calculations for metals and semiconductors using a plane-wave basis set, Comput. Mater. Sci. 6 (1996) 15, https://doi.org/10.1016/0927-0256(96)00008-0.

[17] R. Kingsbury, A.S. Gupta, C.J. Bartel, J.M. Munro, S. Dwaraknath, M. Horton, K. A, Persson Performance comparison of r2 SCAN and SCAN metaGGA density functionals for solid materials via an automated, high-throughput computational workflow, Phys. Rev. Mater. 6 (2022) 013801, https://doi.org/10.1103/PhysRevMaterials.6.013801.

[18] M.C. Gao, C. Niu, C. Jiang, D.L. Irving, in: M.C. Gao, J.W. Yeh, P.K. Liaw, Y. Zhang (Eds.), Chapter 10: Applications of Special Quasi-Random Structures to High-Entropy Alloy in the Book High-Entropy Alloys, Springer, 2016, https://doi.org/10.1007/978-3-319-27013-5.

[19] R. Dronskowski, P.E. Bloech, Crystal orbital Hamilton populations (COHP): energy-resolved visualization of chemical bonding in solids based on density-functional calculations, J. Phys. Chem. 97 (1993) 8617–8624, https://doi.org/10.1021/j100135a014.

[20] R. Nelson, C. Ertural, J. George, V.L. Deringer, G. Hautier, R. Dronskowski, LOBSTER: local orbital projections, atomic charges, and chemical-bonding analysis from projector-augmented-wave-based density-functional theory, J. Comb. Chem. 41 (2020) 1931–1940, https://doi.org/10.1002/jcc.26353.

[21] D.B. Miracle, O.N. Senkov, A critical review of high entropy alloys and related concepts, Acta Mater. 122 (2017), https://doi.org/10.1016/j.actamat.2016.08.081.

[22] A.I. Gusev, Mechanical properties of nonstoichiometric cubic titanium carbide TiC_y, Phys. Chem. Chem. Phys. 23 (2021) 18558–18567, https://doi.org/10.1039/D1CP02697F.

[23] Momma, F. Izumi, VESTA 3 for three-dimensional visualization of crystal, volumetric and morphology data, J. Appl. Crystallogr. 44 (2011) 1272–1276.